Ship-Shaped Offshore Installations

Design, Construction, Operation, Healthcare and Decommissioning

Second Edition

JEOM KEE PAIK
University College London
The International Centre for Advanced Safety Studies (Lloyd's Register Foundation Research Centre of Excellence)

ERRATA

CAMBRIDGE UNIVERSITY PRESS

FATAL ERROR

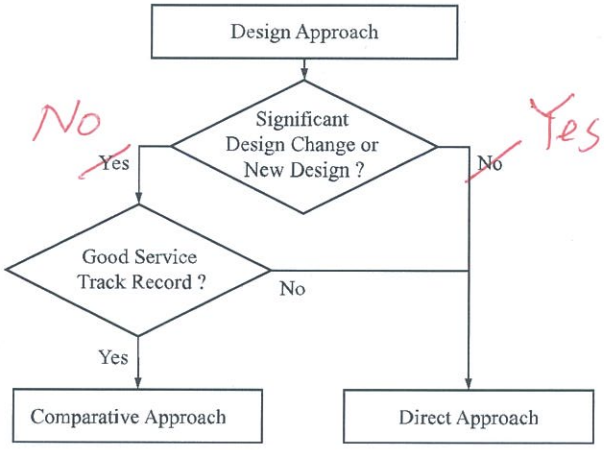

Figure 1.9 Decision tree for the comparative approach versus the direct approach for a new-build design of a ship-shaped offshore installation

Many problems associated with the costs and scheduling of new-build ship-shaped offshore installations result from inadequate project definitions and requirements, which lead to expensive changes being required during the project execution phase. Therefore, front end engineering and design (FEED), which involves substantial engineering analyses, must be performed at the outset of any new-build project, prior to the development of specifications, the issuing of an invitation to tender a package and (usually) the bidding phase. As a new-build project may take three to four years to complete, and its success is dependent on the orchestration and scheduling of a variety of key tasks, such as front-end engineering, the development of a design basis, the determination of performance specifications and detailed specifications, the vetting and selection of candidate yards and contractors, the awarding of the construction contract, the performance of a detailed engineering process, construction, pre-commissioning (dock trials), sea trials, delivery, on-site commissioning and acceptance.

The complexity and sizes of ship-shaped offshore installations have been gradually increasing. Accordingly, aspects of the design, building and operation of each new build may need revision, relative to previous designs, to ensure that a high level of system integrity is achieved. The requirements for the design and construction of a ship-shaped offshore installation differ from those applied to trading tankers, as the former must exhibit excellent on-site reliability over a long operational life, without requiring dry-docking-based repair (described in Section 1.2). Furthermore, ship-shaped offshore installations are much more complex facilities than trading tankers, and their successful construction requires a coordinated effort from all parties, namely the owners, shipyards, topsides integration contractors, hull engineering contractors, classification societies and operators. A detailed engineering process is crucial for the design, construction and commissioning of a new-build project.

This section describes the front-end engineering involved in building a new ship-shaped offshore installation, with a focus on the construction of FPSO units used for

7.3.3 Ultimate Panel Strength Formulation under Lateral Pressure Loads

Bottom stiffened panels of ship-shaped offshore installations are predominantly subjected to lateral pressure loads. A stiffened panel under uniformly lateral pressure loads is modelled as the plate-stiffener combination model under a uniform line load, $q = pb$ (shown in Figure 5.4 with Figure 7.6). In this case, the effectiveness of the attached plating is defined by the 'effective plate breadth' concept resulting from shear lag (defined in Equation (5.3)), unlike the 'effective plate width' concept resulting from non-uniform membrane stress distribution (described in Section 7.2.2).

The ultimate strength of the plate-stiffener combination model under uniformly distributed lateral pressure loads is estimated using the plastic hinge method, as shown in Figure 7.7, for a simple support beam at both ends. The reaction forces at both ends and the bending moment distribution of the beam are calculated as follows:

$$R_A = R_B = \frac{qa}{2}, \quad M = R_A x - \frac{1}{2}qx^2 = \frac{1}{2}qx(a - x), \tag{7.27}$$

where $q = pb$.

The maximum bending moment, M_{max}, at the mid-span, that is, $x = a/2$, is thus obtained as follows:

$$M_{max} = \frac{qa^2}{8}. \tag{7.28}$$

According to the plastic hinge method, a beam reaches the ultimate strength when the maximum bending moment is equal to the plastic bending capacity, M_P, that is,

$$M_{max} = M_P \quad \text{or} \quad q_c = \frac{8M_P}{a^2} \quad \text{or} \quad p_c = \frac{q_c}{b}, \tag{7.29}$$

where q_c is the collapse line load, p_c is the collapse pressure load, M_P is the plastic bending capacity of the plate-stiffener combination model with an effective plating, which is given by (see chapter 2 of Paik (2018) for details)

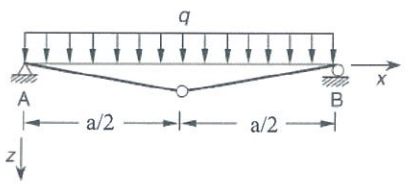

Figure 7.7 Plastic hinge mechanism (collapse mode) of a plate-stiffener combination model under a uniform line load

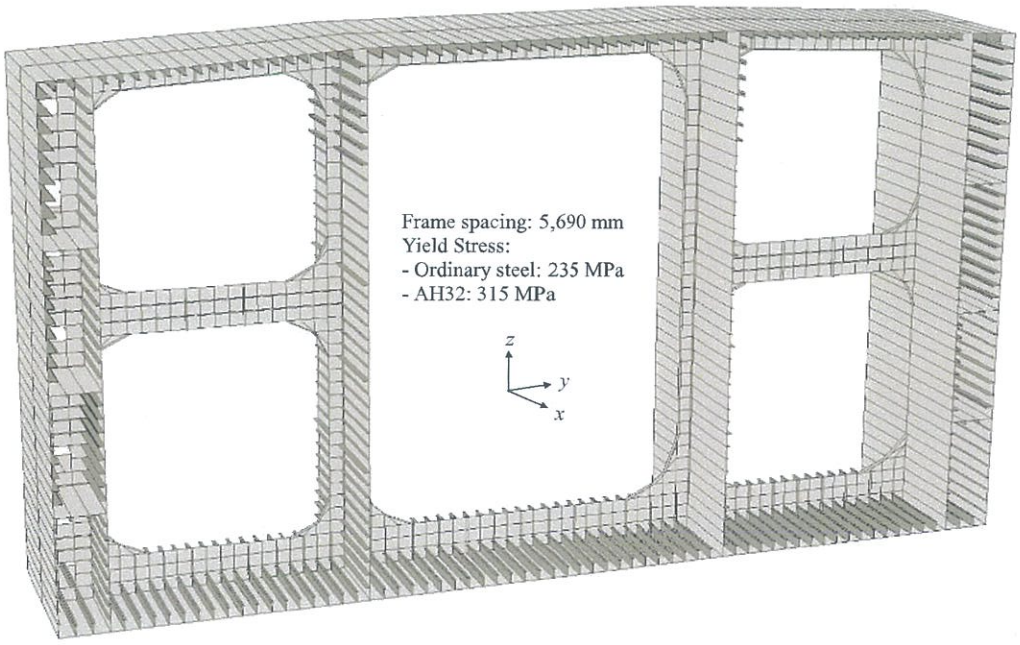

Figure 7.14 The ALPS/HULL two-bay section model (including one transverse frame) of a hypothetical floating production, storage and offloading installation hull

$$\left(\frac{M_V}{M_{Vu}}\right)^{c_1} + \left(\frac{M_H}{M_{Hu}}\right)^{c_2} = 1 \tag{7.40a}$$

$$\left(\frac{M_V}{M_{Vu}}\right)^{c_3} + \left(\frac{F}{F_u}\right)^{c_4} = 1 \tag{7.40b}$$

$$\left(\frac{M_H}{M_{Hu}}\right)^{c_5} + \left(\frac{F}{F_u}\right)^{c_6} = 1 \tag{7.40c}$$

where M_V is the applied vertical bending moment, M_H is the applied horizontal bending moment, F is the applied shearing force, M_{Vu} is the ultimate vertical bending moment, M_{Hu} is the ultimate horizontal bending moment and F_u is the ultimate shearing force. $c_1 - c_6$ are the coefficients, which may be taken as $c_1 = 1.85$, $c_2 = 1.0$, $c_3 = 2.0$, $c_4 = 5.0$, $c_5 = 2.5$ and $c_6 = 5.5$. Also, the ultimate shearing force in Equation (7.40c) may be determined as follows:

$$F_u = \sum_{i=1}^{n} a_i \tau_{ui} \tag{7.41}$$

where a_i is the cross-sectional area of the ith structural element, τ_{ui} is the ultimate shear stress of the ith structural element and n is the total number of structural elements.

Table 7.3. Ultimate bending moments of a hypothetical floating production, storage and offloading installation hull

Method		Ultimate bending moment (GN·m) Hogging	Sagging
USAS-S		23.719	−24.840
ALPS/HULL	Low level*	25.940	−25.474
	Average level	24.815	−23.996
	Severe level	18.987	−17.984

* refers to the level of initial imperfections from Equations (2.11) and (2.12) with Equation (2.14).

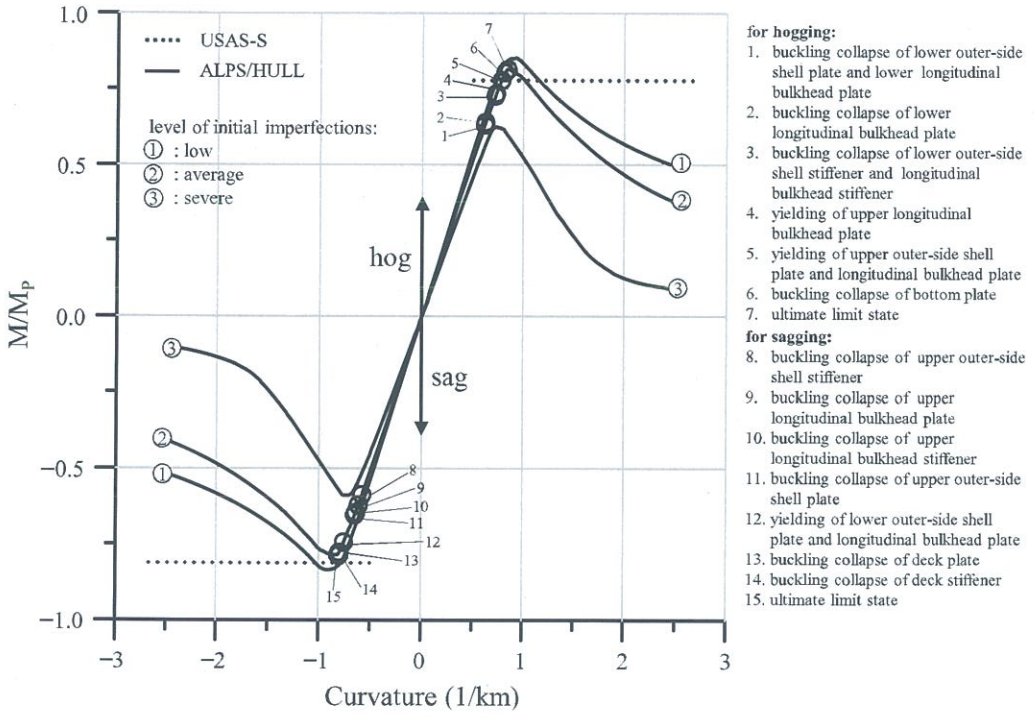

Figure 7.15 Comparison of the progressive collapse behaviour of a hypothetical floating production, storage and offloading installation hull under vertical bending moments

The interaction relation between three hull girder load components is derived by combining the interaction relations between two hull girder load components (see chapter 7 of Paik (2018) for details), as follows:

$$\left(\frac{M_V}{M_{Vu}F_1}\right)^{c_1} + \left(\frac{M_H}{M_{Hu}F_2}\right)^{c_2} = 1 \tag{7.42}$$

where,

$$F_1 = \left[1 - \left(\frac{F}{F_u}\right)^{c_4}\right]^{1/c_3}, \quad \text{and} \quad F_2 = \left[1 - \left(\frac{F}{F_u}\right)^{c_6}\right]^{1/c_5}.$$

7.5 Structural Collapse Triggered by Fracture

The hull structures of ship-shaped offshore installations may be exposed to low (sub-zero) temperatures or to cryogenic conditions owing to the accidental release of liquefied gases, such as liquefied natural gas (LNG) or liquefied hydrogen. Although structural steel is a ductile material (described in Section 2.1), it may fail owing to brittle fracture at a temperature lower than the ductile-to-brittle fracture transition temperature (DBTT), which is a function of the strain rate (loading speed). Whether steel structures undergo ductile or brittle fracture at low temperatures depends on the types of materials and the loading conditions (e.g., quasi-static or impact), among other factors. For example, steel tubes subjected to quasi-static load crush-testing at −60°C underwent ductile fracture (shown in Figure 7.16(a)) (Paik et al. 2011; Park et al. 2015), whereas steel stiffened panels subjected to dropped-object impact testing at −60°C underwent brittle fracture (shown in Figure 7.16(b)) (Kim et al. 2016). Furthermore, a full-scale collapse test of a stiffened steel plate structure under axial-compressive loading revealed that it underwent brittle fracture, thus triggering the ultimate limit states (shown in Figure 7.17) (Paik et al. 2020a, 2020b, 2021a).

Computational models used in the progressive collapse analysis of a hull structure involving fracture behaviour must comprise relevant failure criteria. Numerous fracture criteria associated with extreme loads (rather than repeated fatigue loads) have been formulated, based on the hypothesis that a crack initiates when an equivalent applied stress exceeds the critical stress of a material. These criteria are summarised here.

(a) Maximum principal stress-based fracture criterion

This is one of the simplest criteria, and focuses on the fracture behaviour of brittle materials under predominantly tensile loads. It states that brittle fracture occurs if the largest principal normal stress reaches the ultimate tensile strength (σ_T) of a material, as follows:

$$\text{Max}.(|\sigma_1|, |\sigma_2|, |\sigma_3|) = \sigma_T, \tag{7.43}$$

where σ_1, σ_2 and σ_3 are the principal stress components.

(b) The Coulomb–Mohr fracture criterion

This criterion is used for the analysis of brittle materials that have much greater compressive strength than tensile strength, such as concrete and cast iron. It states that

FATAL ERROR

12.6 Analysis of Computational Results

12.6.1 Model of a Single Engine Striking a Partial Hull Structure

The LS-DYNA (www.lstc.com/products/ls-dyna) computing time for a 1-s simulation using a computer equipped with an Intel® Xeon® CPU E5–2660 V2 (with 20 cores, 20 threads and DDR3 64GB) was 13 h. The results of the impact crashworthiness analysis are used for the safety engineering of sensitive equipment and the nuclear reactor. In the illustrative example involving a single engine striking partial hull structures, the safety of the silo located 4,500 mm inside the outer hull with a double-side width of 3,000 mm is a concern (shown in Figure 12.16). A comparison

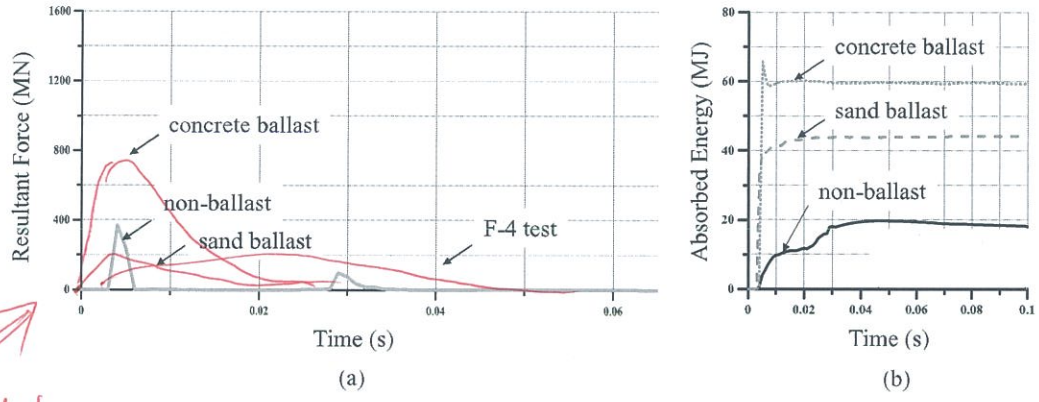

Lines are missing!!

Figure 12.17 Comparison of the impact crashworthiness of hull structures containing no ballast, sand ballast or concrete ballast when impacted by a deformable engine, in terms of (a) the resultant force–time relation and (b) the absorbed energy–time relation

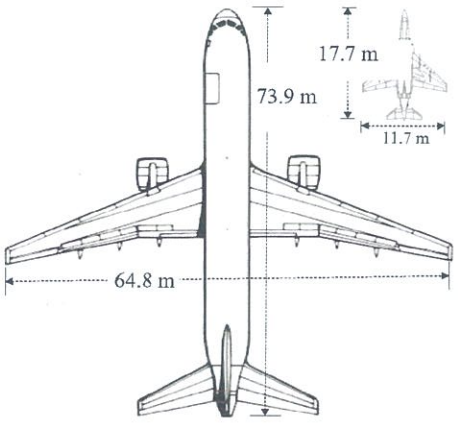

Figure 12.18 A comparison of the body sizes of a McDonnell F-4 Phantom jet fighter and a Boeing 777 passenger jet

$$R = F^a \times C^b < R_a, \tag{13.1}$$

where R is the risk, F is the frequency of the hazard, C is the severity of the consequences, R_a is the acceptable level of risk and a and b are ascending constants (which are often taken as $a = b = 1$). To weight the frequency or consequences, a or b may be allocated a value greater than unity. R is classified into three categories: casualty (fatality), asset damage and environmental pollution (e.g., oil spill or radioactivity spread). To reduce R, either F or C, or both, must be reduced. To meet the risk-acceptance criteria, R must be smaller than R_a, the value of which may vary from one industry to another depending on various factors (e.g., the type of accident, the severity of consequences or sensitivity of the public and media). The task of risk calculation is termed risk assessment, while the task of risk mitigation is termed risk management.

Two approaches are used to calculate risk: the qualitative approach and the quantitative approach. The qualitative approach determines F and C using simple methods, based on past experience and insights. For example, F is scored between 1 (rare) and 5 (almost certain) and C is scored between 1 (negligible) and 5 (severe). Thus, the minimum and maximum scores from Equation (13.1) are 1 and 25, respectively, when $a = b = 1$. If the calculated R is greater than R_a, F or C or both must be managed to reduce R and sufficiently lower the risk of the hazard. Although this approach is simple, it is difficult to incorporate detailed VUCA environmental considerations into qualitative risk assessment and management processes. Figure 13.1 shows a sample calculation of risk using the qualitative appraoch, where the level of calculated risk is termed 'low' for $R \leq 4$, 'medium' for $4 < R \leq 12$ and 'high' for $R > 12$. A low risk is acceptable but must be routinely monitored.

Frequency	Consequence Level: 1 Negligible	2 Low	3 Moderate	4 High	5 Severe
5 Almost certain $>10^{-2}$	5 Medium	10 Medium	15 High	20 High	25 High
4 Likely $10^{-3} - 10^{-2}$	4 Low	8 Medium	12 Medium	16 High	20 High
3 Possible $10^{-4} - 10^{-3}$	3 Low	6 Medium	9 Medium	12 Medium	15 High
2 Unlikely $10^{-5} - 10^{-4}$	2 Low	4 Low	6 Medium	8 Medium	10 Medium
1 Rare $<10^{-5}$	1 Low	2 Low	3 Low	4 Low	5 Medium

Adjust the elevation

Figure 13.1 A sample calculation of risk using the qualitative approach

upper case letter

14.8.2.2 Surface Preparation prior to Coating Application

The durability of a coating is affected significantly by the quality of the surface preparation (Rajput et al. 2019). The requirements for surface preparation vary, and Devanney (2006) is a readable and useful guide to the processes involved. All structural steel must be blasted before coating, as per ISO 8501-1 (Sa3), and immediately shop-primed with an inorganic zinc primer with a minimum dry-film thickness of 20 microns. Sharp edges that result from steel cutting (e.g., with plasma arc torches) must be treated by grinding to form a reasonably smooth arc with a minimum radius of at least 2 mm. Otherwise, paint may stick to these sharp edges and then be removed from a corner by surface tension forces via a phenomenon known as 'pull-back', the magnitude of which is inversely proportional to the radius of a corner. Secondary surface preparation is also required at the block and erection stages. For example, ballast tanks, slop tanks and the bottom half-metres of cargo tanks are re-blasted (as per ISO 8501-1 (Sa3)) to a surface profile of 75–125 microns (as per NACE RP 0287) prior to coating.

Several blasting methods may be used for surface preparation, namely:

- dry (open) grit blasting;
- water-enclosed grit blasting;
- slurry blasting;
- ultrahigh pressure water jetting and
- jet systems.

Dry grit blasting is the most common method used in the shipbuilding industry for the preparation of large surface areas. It is relatively fast and produces good surface profiles for subsequent coating but may not be as efficient or effective for the removal of contaminants, such as salts, from weathered-steel surfaces. Additional treatments, such as washing and drying, may be required in these cases, which increases the cost and work timeline. Open blasting is a noisy and dusty operation that may not be allowed or possible in some areas. Water-enclosed grit blasting is similar to open blasting but includes the use of a water shroud to reduce the amount of dust that is generated. This latter procedure also more effectively removes salt contaminants from the substrate, thus producing a cleaner surface than that achieved with dry blasting. In both methods, run-off water and used grit must be collected, separated and treated before disposal. Slurry-blasting involves combining water and grit at the blast pot, and the resulting mixture serves as the cleaning medium. Ultrahigh pressure water jetting uses water at a pressure greater than 1,500 bar. This technique generates no dust and very effectively removes salts from contaminated surfaces, but it is noisy and slower than dry-grit blasting. Finally, jet systems increase the mechanical impact of cleaning particles on a surface during dry blasting by accelerating an abrasive (that initially travels at a normal velocity from a blast pot) several times before impact. This can provide a higher cleaning efficiency.

As mentioned previously, surface preparation standards require all steel plates, profiles and fittings to be grit-blasted to give a finish equal to ISO 8501-1 (Sa2.5) and

Table 15.6. Required frequency of inspection for ballast water tanks

Year	5	6	7	8	9	10	11	12	13	14	15	16	17	18	19	20
'Good'	S	–	–	I	–	S	–	–	I	–	S	–	–	I	–	S
'Fair' or 'poor'	S	A	A	I	A	S	A	A	I	A	S	A	A	I	A	S

S = special survey; I = intermediate survey; and A = annual survey.

delete

depending on the age of the vessel and other circumstances, such as its history. ASs are typically carried out to determine the general condition of a vessel, and their scope may be altered depending on the circumstances. For instance, the ASs of ballast water tanks are performed when the protective coating is in less than 'good' condition, such that substantial corrosion is present, or if they have no protective coating. Table 15.6 indicates the required frequency of inspection for ballast water tanks. The coating condition is qualitatively characterised as 'good', 'fair' or 'poor', according to IACS Recommendation 87 (IACS 2015) for trading tankers. 'Substantial corrosion' is usually defined as a depth of corrosion wastage that is greater than 75 per cent of the corrosion margin.

Table 15.7 lists the structural parts of trading tankers that must be subjected to close-up surveys, according to the Tanker Structure Cooperative Forum (TSCF) guidelines (TSCF 2019). The quality of a close-up survey determines the confidence that one may place on the results of thickness measurements (gauging). Thus, a special certification scheme has been implemented as part of the ESP to cover the competence of thickness measurement companies. Guidelines for ultrasonic thickness measurements are given by DNV (2016). ESP requirements are often used by default for the inspection of ship-shaped offshore installations, as this is considered good practice or it is mandated by the classification society involved, or for a combination of reasons. However, the operators of offshore installations are increasingly replacing prescriptive ESP requirements with individually developed and tailored risk-based schemes for inspection and maintenance.

15.4.3 Ship Inspection Report Programme

The Ship Inspection Report Programme (SIRE) was initiated in 1993 by the Oil Companies International Marine Forum (OCIMF) as a transparent database of ship conditions to aid the vessel-vetting process. The SIRE requires a detailed questionnaire on the health condition of a ship to be filled out by specially trained inspectors. This questionnaire assesses the systems related to quality, safety and the crew. The results are made available to oil majors and others on a centralised computer database for use in their vessel-vetting processes. The questionnaire also addresses the general condition and repair history of ship hull structures, with reference to the ESP results and ship class and the statutory certificates and status required by the appropriate classification society. An original aim of the programme was to reduce the need for multiple inspections by various vetting interests. The SIRE scheme may also be used

Table 15.7. Structural parts of trading tankers that require close-up survey

Class	Ship age ≤ 5 years	5 years < ship age ≤ 10 years	10 years < ship age ≤ 15 years	Ship age > 15 years
A	One web frame in a ballast wing tank, if any, or a cargo wing tank used primarily for water ballast	All web-frame rings in ballast wing tanks, if any, or a cargo wing tank used primarily for water ballast	All web-frame wings in all ballast tanks, a cargo wing tank, and all remaining cargo wing tanks	Complete a periodical survey as before, plus a deck transverse (if deemed necessary by the classification society)
B	One deck transverse in a cargo oil tank	One deck transverse in each remaining ballast tank, if any, or a cargo wing tank and two cargo centre tanks		
C		Both transverse bulkheads in a wing ballast tank, if any, or a cargo wing tank used primarily for water ballast	All transverse bulkheads in all cargo and ballast tanks	
D	One transverse bulkhead in a ballast tank, a cargo-oil wing tank and a cargo-oil centre tank	One transverse bulkhead in each remaining ballast tank, a cargo-oil wing tank and two cargo-oil centre tanks		
E			One deck and bottom transverse in each cargo centre tank	
F			As considered necessary by the surveyor	

Class A = complete transverse web-frame ring, including adjacent structural members; Class B = deck transverse, including adjacent deck structural members; Class C = complete transverse bulkhead, including the girder system and adjacent members; Class D = transverse bulkhead lower part, including the girder system and adjacent members; Class E = deck and bottom transverse, including the adjacent structural members; and Class F = additional complete transverse web-frame ring.

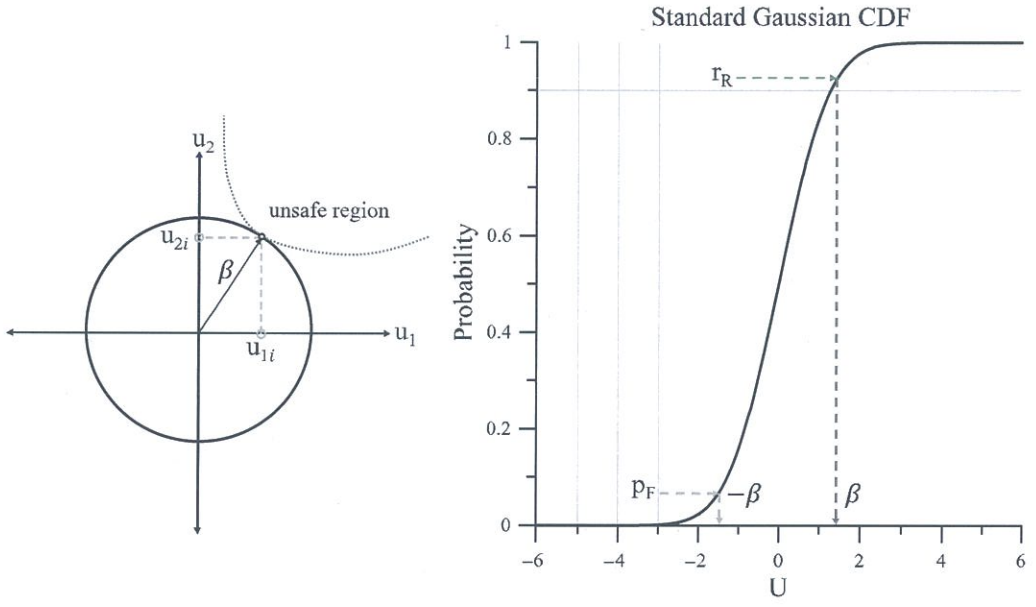

Figure A4.2 Estimation of reliability index in U-shape coordinates associated with standard Gaussian cumulative density function (CDF)

$$p_F = \frac{1}{365 \times \left(\frac{24}{t_s}\right)} \frac{1}{T_R} \tag{A4.1}$$

where p_F is the probability of failure, which is taken as $p_F = 1 - r_R$, T_R is the return period in years, and t_s is the time interval of recorded wave data. r_R is the reliability associated with the corresponding return period.

A joint distribution of the significant wave height H_s and the average zero-up-crossing wave period T_z is considered (shown in Figure A4.3).

$$f(H_s, T_z) = f_{H_S}(H_s) f_{T_Z|H_S}(T_z|H_s) \tag{A4.2}$$

where $f(H_s) = \frac{C_2}{C_1}\left(\frac{H_s - C_3}{C_1}\right)^{C_2 - 1} \exp\left[-\left(\frac{H_s - C_3}{C_1}\right)^{C_2}\right]$, $f_{T_Z|H_Z}(T_z|H_s) = \frac{1}{T_z \sigma \sqrt{2\pi}} \exp\left[-\frac{(\ln T_z - \mu)^2}{2\sigma^2}\right]$, C_1, C_2 and C_3 are the coefficients of Weibull function. μ is the mean and σ is the standard deviation and both are functions of the significant wave height that may be expressed by regression analysis as $\mu = a_1 + a_2 H_s^{a_3}$, $\sigma = b_1 + b_2 e^{b_3 H_s}$ (shown in Figure A4.4).

The reliability index β is determined from the inverse of the cumulative probability function using the standard Gaussian distribution (shown in Figure A4.2).

$$\Phi^{-1}(r_R) = \beta = \sqrt{u_{1i}^2 + u_{2i}^2} \tag{A4.3}$$

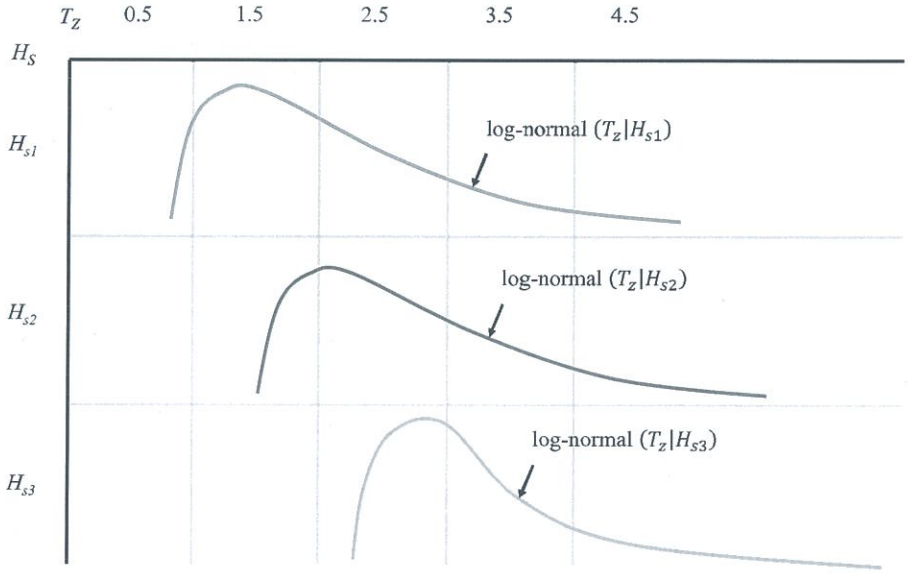

Figure A4.3 Wave scatter diagram for the development of a joint distribution between H_s and T_z

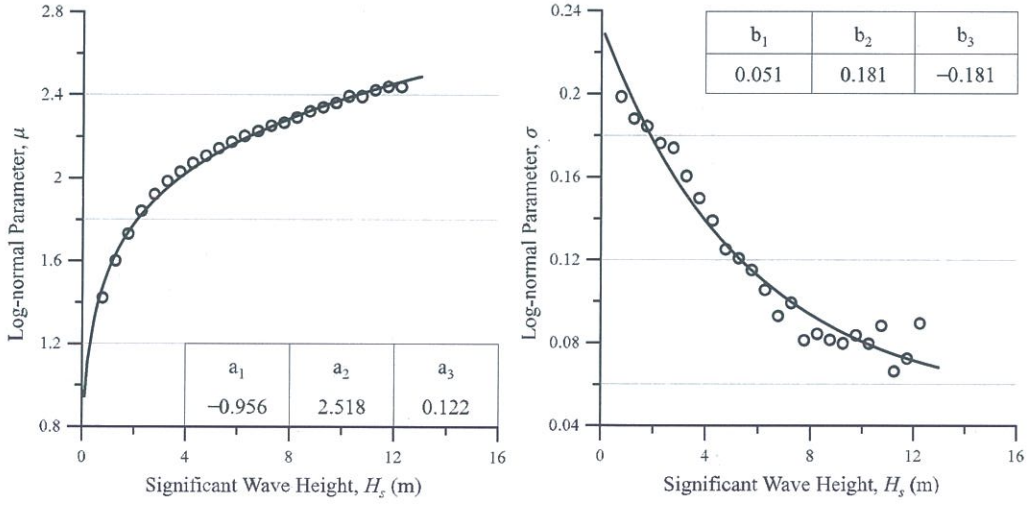

Figure A4.4 A schematic of the regression analysis

where Φ is the cumulative probability function of standard Gaussian distribution. The relation between physical variables and U-space variables is given by

$$T_i = \mathrm{CDF}_{T_Z|H_S}{}^{-1}\{\Phi(u_{1i})\}, \quad H_i = \mathrm{CDF}_{H_S}{}^{-1}\{\Phi(u_{2i})\} \tag{A4.4}$$

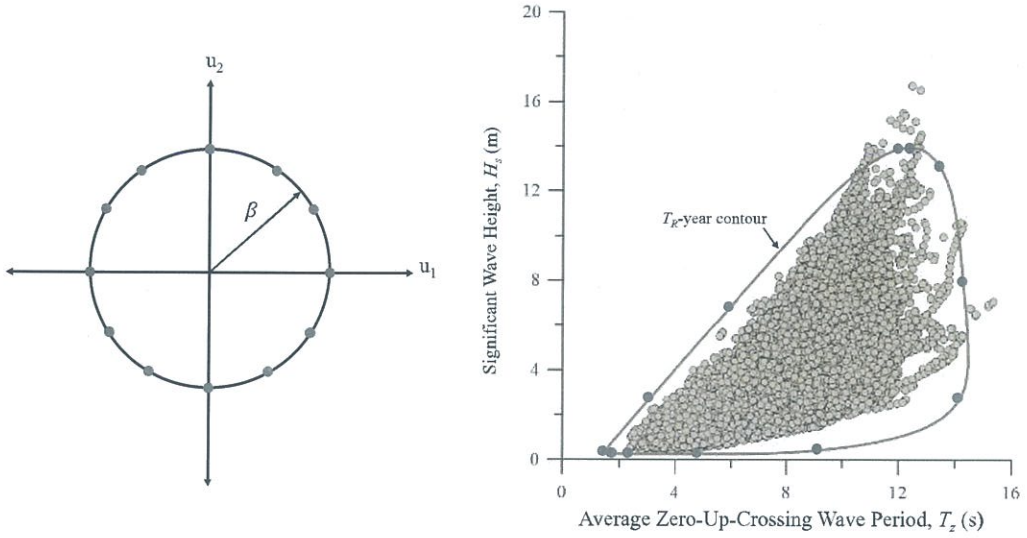

Figure A4.6 Drawing of the wave contour in the H_s-T_z coordinate

where T_i is the physical variable for the wave period and H_i is the physical variable for the significant wave height. CDF is the cumulative density function in the U-space, which is used for the transformation of variables (shown in Figure A4.5).

CDF for Weibull function:

$$\text{CDF} = 1 - \exp\left\{-\left(\frac{H_s - C_3}{C_1}\right)^{C_2}\right\} \tag{A4.5a}$$

CDF for log-normal function:

$$\text{CDF} = \frac{1}{2}\text{erfc}\left(-\frac{\ln T_z - \mu}{\sigma\sqrt{2}}\right) \tag{A4.5b}$$

where erfc is the complementary error function. If the transformation of variables in U-space coordinates to the H_s-T_z coordinate is completed for a given return period, the extreme wave contour can be drawn (shown in Figure A4.6).